RSC Advances

This is an *Accepted Manuscript*, which has been through the Royal Society of Chemistry peer review process and has been accepted for publication.

Accepted Manuscripts are published online shortly after acceptance, before technical editing, formatting and proof reading. Using this free service, authors can make their results available to the community, in citable form, before we publish the edited article. This *Accepted Manuscript* will be replaced by the edited, formatted and paginated article as soon as this is available.

You can find more information about *Accepted Manuscripts* in the Information for Authors.

Please note that technical editing may introduce minor changes to the text and/or graphics, which may alter content. The journal's standard Terms & Conditions and the Ethical guidelines still apply. In no event shall the Royal Society of Chemistry be held responsible for any errors or omissions in this *Accepted Manuscript* or any consequences arising from the use of any information it contains.

ROYAL SOCIETY OF CHEMISTRY

www.rsc.org/advances

New insight into the promotion effect of Cu doped V_2O_5/WO_3-TiO_2 for low temperature NH_3-SCR performance

Meiqing Shen,[a,b,c] Chenxu Li,[a] Jianqiang Wang,[*a] Lili Xu,[a] Wulin Wang [a] and Jun Wang[*a]

[a] Key Laboratory for Green Chemical Technology of State Education Ministry, School of Chemical Engineering & Technology, Tianjin University, Tianjin 300072, PR China

[b] Collaborative Innovation Center of Chemical Science and Engineering (Tianjin), Tianjin 300072, PR China

[c] State Key Laboratory of Engines, Tianjin University, Tianjin 300072, PR China

* Corresponding author: Jun Wang, Jianqiang Wang

Postal address:

School of Chemical Engineering and Technology, Tianjin University, 92 Weijin Road, Nankai District, Tianjin 300072, China

Email: jianqiangwang@tju.edu.cn; wangjun@tju.edu.cn

Tel. /Fax. : (+86) 22-27407002

RSC Advances Accepted Manuscript

Abstract

The promotion effect of Cu on V/WTi catalyst for the selective catalytic reduction of NO_x by NH_3 was investigated in the temperature range of 150-400 ˚C. The Cu addition shows a superior NH_3-SCR performance in comparison with V/WTi sample. The catalysts were characterized by XRD, Raman, EPR, H_2-TPR, XPS, and *in situ* DRIFTS techniques. Obtained results reveal the Cu oxides in close proximity to V oxides on the surface facilitate the formation of double redox couples of V^{5+}/V^{4+} and Cu^{2+}/Cu^{+}, which may play a critical role in the superior NH_3-SCR performance. The electronic interactions caused by the redox cycle of $Cu^{2+}+V^{4+}\leftrightarrow V^{5+}+Cu^{+}$ could significantly improve the redox properties of vanadium species, which is beneficial for the activation of NH_3 species bound to vanadium species. Moreover, the redox cycle of $Cu^{2+}+V^{4+}\leftrightarrow V^{5+}+Cu^{+}$ induces the formation of high-activity nitrates species adsorbed on Cu species. The kinetic analysis reveals that the Cu doping induces the decrease of activation energy (Ea) of NH_3-SCR.

RSC Advances Accepted Manuscript

1. Introduction

Nitrogen oxides (NO_x), are one of the most dangerous air pollutants that cause acid rain and photochemical smog, as well as directly do harm to human health [1]. The selective reduction of NO_x by NH_3 is one of the most efficient NO_x emission control technologies [2]. V_2O_5-WO_3/TiO_2 has been a well-known NH_3-SCR catalyst and shows optimum performance in only within a narrow temperature window of 300-400 ˚C [3]. Under the condition of low-load operation, the temperature of exhausted gas cannot reach to the lowest operation temperature, causing the SCR denitrification system not operation. This phenomenon could account for the lower flue gas temperature leading to NH_4HSO_4 deposited on the catalyst surface [4], resulting in the blockage of catalyst pore channels and catalyst deactivation. These problems need to be settled currently for most coal power plant. Hence, it is urgent to develop a novel NH_3-SCR catalyst with excellent NO_x conversion at low temperature to avoid the problems associated with the existing commercial system, especially for the coal power plant [5-7].

In the past decades, many researchers have been dedicated to improve the low-temperature activity of V_2O_5-based NH_3-SCR catalysts. Gao et al. [8] revealed that Fe_2O_3 additive in V_2O_5-WO_3/Fe_2O_3/TiO_2 improved the NO decomposition due to the oxidation of NO to NO_2 by Fe_2O_3. Liu et al. [9] pointed out the Mn addition significantly enhanced the activity of V_2O_5/TiO_2 catalyst for NH_3-SCR below 400 ˚C owing to the synergistic effect of the redox cycle (Mn^{4+}+V^{4+}↔V^{5+}+Mn^{3+}). These additives can not only serve as “structure” promoter but also play a “chemical” role in promoting the redox properties and influencing other intrinsic chemical states of the

RSC Advances Accepted Manuscript

active vanadium species, including oxidation state and coordination circumstance, which is consistent with the promotion effect of WO_3 or MoO_3 [10, 11]. Recently, highly dispersed amorphous copper oxides [12] have been attractive due to the excellent performance in NO_x conversion. Aritani et al. [13] reported CuO-TiO_2 showed high activity even at relatively low temperature in the NH_3-SCR process. Ettireddy et al. [7] developed the Cu/TiO_2 catalyst that presented superior de-NO_x performance at the low temperature under industrial relevant condition. The low temperature performance is associated with the remarkable surface Lewis acidic sites and the existence of redox cycle between Cu^{2+} and Cu^{+}. However, limited information is available to regard the promotional effect of copper oxides on the V_2O_5–WO_3/TiO_2 catalysts for NH_3-SCR active, especially the detail investigations focusing on further understanding the relationship among the "composition-structure-property" remain unreported.

It is well received that the redox property of vanadium species is principal factor governing activity and that this reaction may involve primarily the coordinated ammonia species on Lewis acid sites [10, 14, 15]. Therefore, it is possible to improve the performance of V/WTi catalyst at low temperature by adding Cu. Meanwhile, it seeks to further understand the structure-performance correlation of copper oxide addition on the V/WTi catalyst. The V/WTi was first prepared by traditional incipient wetness impregnation method, and then, Cu was added to gain the V(Cu)/WTi catalyst with the same method. The promoting effect of Cu on the SCR active was evaluated and the structure-performance correlation on NH_3-SCR performance was investigated. Moreover，the mechanism study was conducted by *in situ* DRIFTS techniques and

RSC Advances Accepted Manuscript

kinetic analysis to elucidate the cause of Cu influencing the NH_3-SCR performance. Finally, a mechanism of NH_3-SCR over V(Cu)/WTi catalyst at low temperature is proposed to further understand the promotion effect.

2. Experimental

2.1 Catalysts preparation

The CuO (molar ratio Cu/V=1:1) modified V_2O_5/WO_3-TiO_2 catalyst with 1wt % V_2O_5 was prepared by the traditional incipient wetness impregnation method. Commercial support (DT-52), was obtained from Millennium Inorganic Chemicals Inc. The complex of $VO(CO_2)_2$ was prepared by reacting calculated amount of V_2O_5 powder with appropriate amount of oxalic acid liquid (1 M) with continuous stirring at 70 ˚C for 30 min. Subsequently, the desired quantity of WTi powder was added into the mixed solution and stirred at 70 ˚C for 1 h. This mixture was statically dried overnight at 100 ˚C. The V(Cu)/WTi and Cu/WTi were prepared by the same method with dissolving a desired amount of $Cu(NO_3)_2 \cdot 5H_2O$ into the aqueous solutions, and then the desired amount of dried V/WTi powder without calcination and WTi added into the mixed solutions and stirred 1h, then dried overnight at 100 ˚C and calcined at 600 ˚C for 5 h.

2.2 Catalysts characterization

Powder X-ray diffraction (XRD) was performed on Bruker D8 Advance TXS employing Cu Kα radiation (λ=0.15418 nm). The XRD pattern was collected from

RSC Advances Accepted Manuscript

20^{o} to 80^{o} with the step size of 0.02^{o}. The mean crystallite sizes of titania are calculated using Scherer equation. The Nitrogen adsorption-desorption isotherms of the samples were determined at -196 ˚C by V-Sorb 2800TP, and the corresponding pore size distribution curves were calculated from branches by the BJH method. The BET surface area is calculated from the Brunauer-Emmett-Teller (BET) method. The samples were degassed for 5 h at 300 ˚C in N_2 before measurement.

Electron paramagnetic resonance spectroscopy (EPR) was performed with a Bruker Model A320 instrument in a rectangular ER 4102st cavity. Prior to analysis, the samples were pretreated for 5 h at 300 ˚C, and then the EPR spectra was recorded at room temperature and atmospheric pressure.

Hydrogen temperature-programmed reduction (H_2-TPR) was conducted using 0.1 g catalysts. The samples were pretreated with 5 % O_2/N_2 (30 ml min^{-1}) at 500 ˚C for 1 h and then cooled down to room temperature in N_2. The samples were elevated in 5 % H_2/N_2 (30 ml min^{-1}) from 50 to 900 ˚C at a ramping rate of 10 ˚C min^{-1} while the consumption of H_2 was recorded continuously using TCD.

The X-ray photoelectron spectroscopy (XPS) was recorded on a PHI-1600 ESCA system. All binding energies were calibrated internally by the carbon deposit C 1s binding energy (BE) at 284.8 eV.

The temperature-programmed desorption (TPD) of NO+O_2 was performed using a Fourier Transform Infrared spectrometer (MKS-2030). Prior to TPD, 0.2 g samples were pre-treated with 5 % O_2/N_2 (333 ml min^{-1}) at 500 ˚C for 0.5 h and then cooled down to 50 ˚C. For NO+O_2-TPD, the samples were saturated with a 500 ppm NO+5%

RSC Advances Accepted Manuscript

O_2/N_2 for 1 h, followed by N_2 purge for another 1 h. The temperature was then raised up from 50 ˚C to 500 ˚C at a 10 ˚C min^{-1} ramping rate.

In situ diffuse reflectance Infrared Fourier transform spectra of adsorption species were performed on Nicolet 6700 FTIR equipped with a MCT detector cooled by liquid N_2 at a resolution of 4 cm^{-1}, averaging 10 scans for each spectrum. Diffuse reflectance experiments were performed *in situ* in a commercial high temperature chamber (Thermofisher) fitted with a ZnSe window. Prior to reactant gas (NH_3 or NO) chemisorption, the samples were initially treated with 10 % O_2/N_2 (50 ml min^{-1}) at 500 ˚C for 30 min, and then the samples were cooled down to the target temperature. The samples were subsequently flushed under N_2 for 1 h to remove any adsorbed impurities for background collection. Then the gas containing 3000 ppm NH_3 or 3000 ppm NO+5 % O_2 in N_2 (50 ml min^{-1}) passed through the sample at the target temperature for 45 min. *In situ* DRIFTS spectra were collected after purging the weakly adsorbed gas molecules. *In situ* DRIFTS spectra for NO, NH_3 and O_2 co-adsorption were collected at the similar conditions as NO chemisorption, where 3000 ppm NO and 3000 ppm NH_3 in 5% O_2+N_2 were introduced to the system.

2.3 Activity measurement

The catalytic activity measurement for the reduction of NO by NH_3 (NH_3-SCR) was carried out in a quartz reactor with 0.2 g catalysts (60-80 mesh) with 0.8 g of quartz (60-80 mesh). The temperature was monitored by a type K thermocouple inserted into the center of the catalyst. The concentrations of NO, NO_2, N_2O, H_2O and

RSC Advances Accepted Manuscript

NH_3 were measured using a Fourier Transform Infrared spectrometer (MKS-2030) equipped with a 5.11 m gas cell. The gas flow rates in all experiment were controlled at 333 ml min^{-1} using mass flow controllers. Prior to experiments, the catalysts were pre-treated at 500 ˚C for 30 min under 5% O_2/N_2. The NO_x conversion was measured from 100 ˚C to 500 ˚C at a ramp rate of 10 ˚C min^{-1}. The reaction gas mixture contained 500 ppm NH_3, 500 ppm NO, 4 % H_2O, 5% O_2, and the balance of N_2 at gas hourly space velocity (GHSV=10,000 h^{-1}). The NO_x conversion was calculated using the following equation:

$$NO_x conversion(\%) = \frac{NO_{xinlet} - NO_{xoulet}}{NO_{xinlet}} \times 100\% \quad (1)$$

$$NO_x = NO + NO_2 \quad (2)$$

2.4 Kinetic measurement

The kinetic tests were performed in a differential reactor, using 25 mg (80-100 mesh) of 75 mg of quartz sands (80-100 mesh). To avoid the diffusion effect, the experiment was carried out under steady-state conditions at high GHSV (300,000 h^{-1}). The samples were pre-treated in 5 % O_2/N_2 at 500 ˚C for 30 min before the kinetic experiments. The kinetic steady-state measurements with a gas composition of 500 ppm NH_3, 500 ppm NO and 5% O_2 were performed between 220 and 280 ˚C. The kinetic parameters for the NO conversion were generally considered to be a first order reaction [16-18]. The rate constant (k) can be calculated as：

$$k = -\frac{F_0}{[NO]_0 W_{cat}} \ln(1 - X) \quad (3)$$

RSC Advances Accepted Manuscript

$$k = Ae^{\left(\frac{-Ea}{RT}\right)} \quad (4)$$

Where k is the reaction rate constant (ml g^{-1} s^{-1}), F_0 is the molar NO feed rate (mol min^{-1}), $[NO]_0$ is the molar NO concentration (mol min^{-1}) at the inlet, W_{cat} is the catalyst weight (g), X is the NO conversion (%), A is the pre-exponential factor, Ea is the apparent activation energy (J mol^{-1}), R is the gas constant (8.314 J mol^{-1} K^{-1}) and the T is the temperature (K).

3. Results

3.1 NH_3-SCR performance

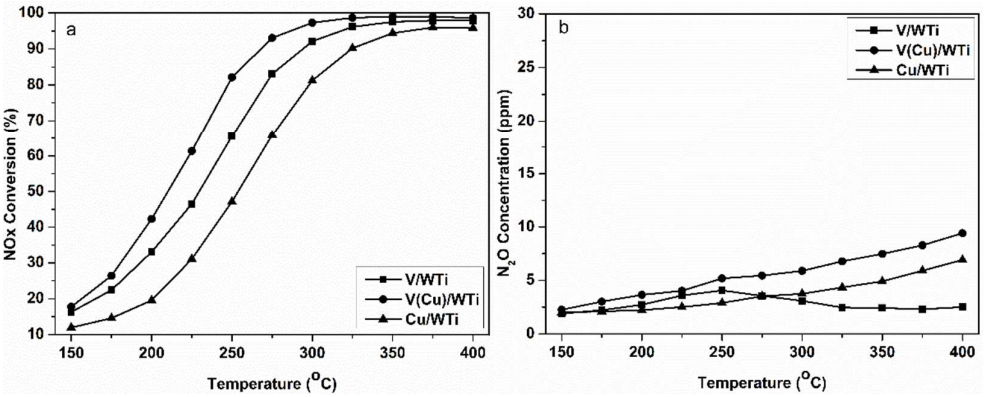

Fig.1 NH_3-SCR evaluation on V/WTi, V(Cu)/WTi and Cu/WTi catalysts as a function of temperature. (a) NO_x conversion (b) N_2O generatio

As shown in Fig.1, NH_3-SCR performance of these catalysts follows the order: V(Cu)/WTi>V/WTi>Cu/WTi. Although, the V/WTi sample exists a better NH_3-SCR activity than Cu/WTi as a reference sample in the whole temperature range, NO_x conversion of this sample is still less than 65 % below 250 ˚C. While V(Cu)/WTi expresses a superior NH_3-SCR performance in comparison with V/WTi and the

RSC Advances Accepted Manuscript

temperature window shifts toward lower temperature. At 250 ˚C the NO_x conversion reaches 84%, much higher than the 65 % of V/WTi and the 46 % of Cu/WTi. The result clear shows that the co-existence of Cu and V could significantly enhance NH_3-SCR activity at low temperature. Under the reaction condition without H_2O, the NH_3-SCR performance showed in Fig.S2 for all catalysts is improved at low temperature, and the similar inhibiting effect of H_2O on activity has been observed by others [16], which is attributed to the competitive adsorption of H_2O on the vanadia sites leading to a reduction in the number of sites available for the adsorption of reagent. While the activity of three catalysts follows the same sequence of V(Cu)/WTi>V/WTi>Cu/WTi under the reaction condition with or without H_2O.

3.2 Characterization

3.2.1 Phase composition and surface area

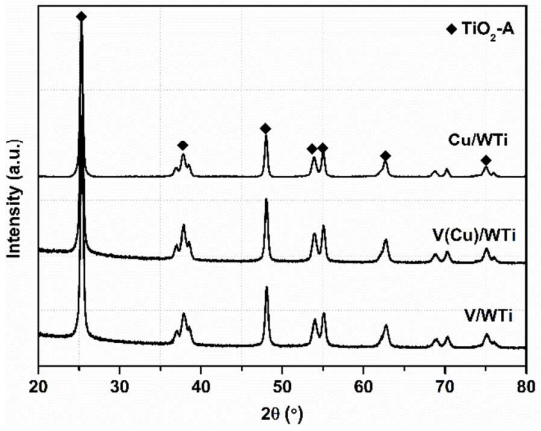

Fig.2 XRD patterns of various catalysts

RSC Advances Accepted Manuscript

Table 1 Textural and structural properties of the catalysts.

Samples	[a]S_{BET} ($m^2 g^{-1}$)	[b]V_{BJH} ($cm^3 g^{-1}$)	[c]D_{BJH} (nm)	TiO_2 crystalline size(nm)	Lattice Parameters a=b(Å)	Lattice Parameters c(Å)	Cell volume ($Å^3$)
V/WTi	41	0.291	19.0	20.4	3.784	9.500	136.0
V(Cu)/WTi	37	0.281	20.1	21.1	3.787	9.508	136.4
Cu/WTi	37	0.290	20.0	21.6	3.786	9.513	136.4

[a]BET surface area of the samples. [b]BJH desorption cumulative volume of pores. [c]BJH desorption average pore diameter (4V/A).

XRD results are showed in Fig.2, and the crystalline sizes, lattice parameters and cell volume are listed in Table 1. These samples all exhibit the typical anatase phase of TiO_2, but no CuO and V_2O_5 diffractions are observed. It indicates that both CuO and V_2O_5 are well dispersed on the surface of TiO_2 as highly amorphous states or formed crystallites are too small to be detected. As showed in Table 1, besides the S_{BET} and V_{BJH}, their crystalline sizes, lattice parameters and cell volume also remain the same level, which suggests almost no or little effect on the support crystal structure with the introduction of CuO and V_2O_5. The theoretical surface density of vanadium on V/WTi and V(Cu)/WTi is 2.7 μmol/m^2 and 2.9 μmol/m^2, which is clearly less than the monolayer coverage (13.2 μmol/m^2) [19]. So, the vanadium species can be well dispersed on the support with the Cu doping. Moreover, it can be well explained by the Raman spectra. As shown in Fig.S2, the Raman vibration mode of

RSC Advances Accepted Manuscript

anatase TiO_2 can only be observed over V(Cu)/WTi and V/WTi without any signals for other metal, especially no bands ascribed to polymeric metavanadate species observed. Therefore, it has concluded that the V and Cu species can be highly dispersed on the support.

3.2.2 EPR

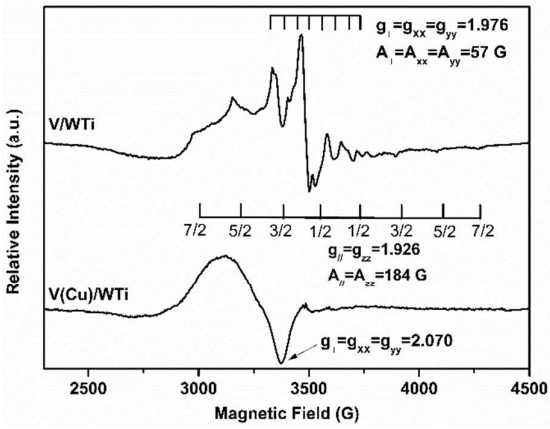

Fig.3 EPR spectra of V/WTi and copper-containing V/WTi at room temperature after they were evacuated for 5 h at 300 ˚C and sealed off.

EPR spectra of the samples are displayed in Fig.3. Tetravalent vanadium exists a quite complex electron resonance spectrum, which is due to the high number of hyperfine lines arising from the interaction of the unpaired electron with the ^{51}V nucleus and the anisotropy of both g and A tensors [20], therefore their parameters may not be exactly calculated. The parameters of anisotropic g factors and hyperfine splitting constants for V/WTi are as follow: $g_{//}=1.926 \pm 0.002$, $g_{\perp}=1.976 \pm 0.002$, $A_{//}=184 \pm 2$ G, and $A_{\perp}=57 \pm 2$ G values, which arises from the isolated, axially symmetric VO^{2+} species in square-pyramidal and/or octahedral coordination [10, 20-22].

RSC Advances Accepted Manuscript

The broad isotropic singlet can be observed, which is assigned to the clustered V-O-V clusters [10]. In addition, the type hyperfine structure of the isolated VO^{2+} species exhibiting a broad signal indicates the presence of V^{4+} in V/WTi, which has been reported by others [14]. The spectrum of V(Cu)/WTi, however, is much smaller, actually almost no hyperfine structure to be discerned, which may be due to the presence of copper suppressing stable isolated V^{4+} formation. Only the EPR signal corresponding to octahedral isolated Cu^{2+} presets $g_{\perp}$= 2.070±0.002 appears [23]. This result can be attributed to an affinity of interaction between surface copper and vanadium oxides. Thus the quasi-free electrons of the V^{4+} species can be captured by the copper component in the vicinity of surface vanadium oxide species, causing the concentration less than the limiting value, which results in the signals of the V^{4+} species too weak to be observed. This conclusion will be further confirmed by the following H_2-TPR and XPS analysis.

3.2.3 H_2-TPR

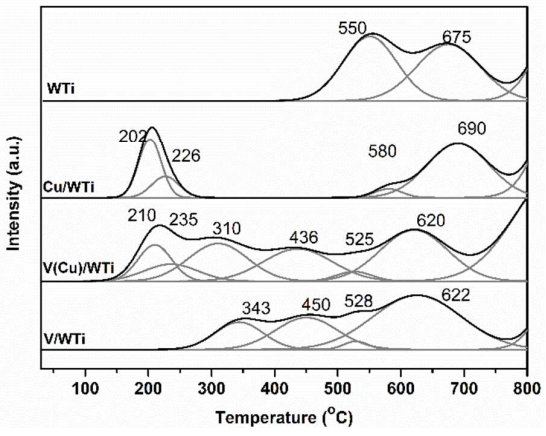

Fig.4 The H_2-TPR result of the catalysts

RSC Advances Accepted Manuscript

240 **Table 2** H_2-temperature programmed reduction.

samples	Reduction peaks temperature (˚C)					
	Cu		V		SO_4^{2-}	Support (W and Ti)
	T_1	T_2	T_1	T_2	T_1	T_1
WTi	-	-	-	-	550	675
V/WTi	-	-	343	450	528	625
V(Cu)/WTi	210	235	310	436	525	620
Cu/WTi	202	226	-	-	580	690

241

242 **Table 3** H_2 consumption of the obtained samples.

samples	Cu^{2+}/Cu^{+}	V^{5+}/V^{4+}	Total H_2 consumption of V and Cu (mmol/g)
V/WTi	-	0.66	1.42
V（Cu）/WTi	1.32	1.00	1.90
Cu/WTi	2.30	-	1.46

243

244 Temperature-programmed reduction (H_2-TPR) experiments were conducted to
245 further investigate the effect of copper modification on the reduction behavior and the
246 results are presented in Fig.4. The support exhibits two major reduction peaks at 550
247 ˚C and 675 ˚C, which can be assigned to the reduction of some sulfate species existing

RSC Advances Accepted Manuscript

on the surface of support [24, 25] and the well dispersed tungsten species oxide and TiO_2 support [26]. The V/WTi catalyst shows two new reduction peaks at 343 ˚C and 450 ˚C ascribed to the stepwise reduction of V^{5+} and V^{4+} [25, 27, 28], and the peak of support TiO_2 and tungsten oxide is clear shifted to lower temperature, which can be an indication of the strong interaction between V and support. The reduction temperature of vanadium species is obviously lower that is accounted for the V-O-Ti interaction [27], which is accorded with the lower reduction temperature of the support. The shoulder peak at 528 ˚C is remarkably smaller than that of the support, corresponding to the decomposition of the sulfate species during the calcination process [10], which can be observed over other two catalysts. In presence of Cu, the new overlapped peaks deconvoluted two sub-peaks at 210 ˚C and 235 ˚C are attributed to the reduction of Cu^{2+} and Cu^{+} [29, 30], which shifts to higher temperature, compared to the peaks at 202 ˚C and 226 ˚C for Cu/WTi. Meanwhile, the reduction temperature of vanadium species clear shifts to lower temperature (310 ˚C and 436 ˚C). It suggests the reducibility of vanadium species is significantly improved by Cu oxide. The last broaden peak due to the support is just like the V/WTi, which means that the interaction between the Cu and the W or Ti can be very weak. The signals have been fitted with Gaussian lines to assess the H_2 consumptions for the individual species, and the results of quantitative analysis are displayed in Table 3. The amount of H_2 consumption due to V reduction on V/WTi is 1.42 mmol/g and Cu on Cu/WTi is 1.46 mmol/g, while the total H_2 consumption due to both Cu and V on V(Cu)/WTi is 1.90 mmol/g that is lesser than the sum of V/WTi and Cu/WTi samples. Meanwhile, the H_2

RSC Advances Accepted Manuscript

consumption ratio of V^{5+}/V^{4+} increases with the ratio of Cu^{2+}/Cu^{+} decreasing shown in Table 3, which suggests larger amounts of easily reduced V^{5+} species formation on the Cu modified V/WTi sample, which is highly consistent with the EPR. The results strongly indicates that the synergistic interaction between V and Cu exists in V(Cu)/WTi catalyst, which greatly enhances the reduction potential of vanadium species. The synergistic interaction will be expounded in detail with the following discussion.

3.2.4 XPS

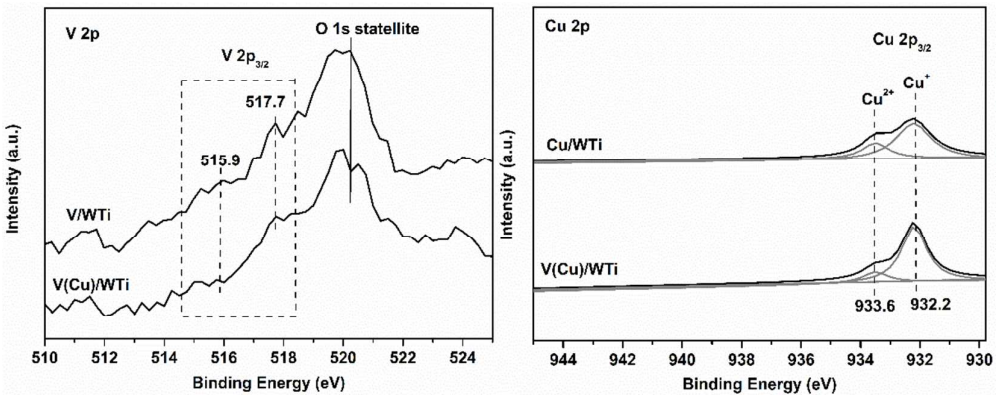

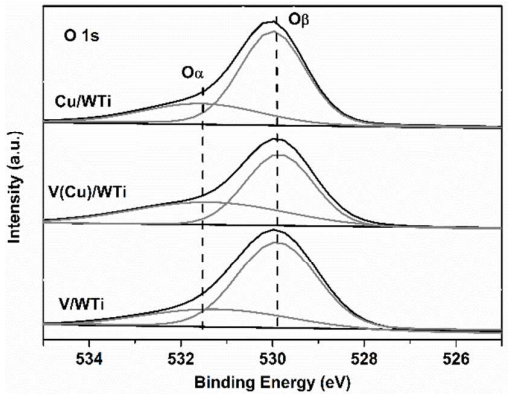

Fig.5 XPS spectra of the obtained samples: V 2p, Cu 2p and O 1s.

RSC Advances Accepted Manuscript

Table 4 The surface compositions of the obtained samples.

Samples	Surface Atomic concentration				Surface Atomic ratio	
	Ti (at.%)	W (at.%)	Cu (at.%)	O (at.%)	$Cu^{2+}/(Cu^{2+}+Cu^{+})$ (%)	$O_\alpha/O_\alpha+O_\beta$ (%)
V/WTi	21.15	5.02	-	73.84	-	30.83
V(Cu)/WTi	19.47	4.65	0.88	75.00	15.83	42.85
Cu/WTi	22.96	5.00	0.93	71.11	24.18	27.09

XPS analysis for the samples are illustrated in Fig.5 and Table 4. As shown in Fig.5 (V 2p), the vanadium oxide species in different chemical state can be identified by the position of the V $2p_{3/2}$ level. The V $2p_{3/2}$ peak within the range reported for V^{5+} (517.0-517.8 eV) and V^{4+} (515.6-516.1 eV) is very weak and impeded by the near O 1s satellite peak (520.3 eV). The results indicate the vanadium species are highly dispersed and located on the support in accord with the XRD and Raman analysis, and the V surface concentration is too low to quantitatively analyze. However the weak shoulder peaks exhibiting at 515.9 eV and 517.7 eV ascribed to V^{4+} and V^{5+} can be detected [31-33], suggesting that the redox couple V^{5+}/V^{4+} exists on the catalysts which is in good agreement with our H_2-TPR and EPR.

The result of Cu 2p is shown in Fig.5 (Cu 2p). The binding energies of Cu $2p_{3/2}$ and Cu $2p_{1/2}$ peaks are located at 932.6 eV and 952.4 eV. The catalysts with low

RSC Advances Accepted Manuscript

298 copper oxide loading exhibit a main center at 932.2 eV and a weak peak at 933.6 eV,
299 which are the characteristics of Cu^{+} and Cu^{2+} species, respectively [34]. For Cu/WTi and
300 V(Cu)/WTi samples, the shake-up peak is very weak, indicating that the main copper
301 specie is the Cu^{+}. The relative percentage of Cu^{2+} can be determined by the area ratio
302 of the corresponding characteristic peaks, and listed in Table 4. In comparison with
303 the Cu/WTi, the percent of Cu^{2+} on the V(Cu)/WTi sample is much lower, which is
304 mainly owing to the redox cycle of $Cu^{2+}+V^{4+}\leftrightarrow V^{5+}+Cu^{+}$ shifting to the right, that is to
305 say the electrons can conduct from V^{4+} to Cu^{2+} resulting in the higher amount of Cu^{+}
306 and V^{5+} formed, which is well agreed with the H_2-TPR and EPR results. In addition,
307 the redox couple of Cu^{2+}/Cu^{+} can reduce the surrounding electron clouds density of
308 the vanadium species [35], promoting the electron transformation between the vanadium
309 species and reagent, thus facilitating the reducibility of vanadium species as shown in
310 H_2-TPR profile.

311 The O 1s ionization of the XPS spectrum features is numerically fitted with two
312 components: the first peak at 529.7 eV is attributed to the lattice oxygen (denoted as
313 O_β) and the one at 531.2 eV is ascribed to the surface adsorbed oxygen (denoted as O_α)
314 such as O_2^{2-} or O^{-} assigned to the defect oxide or surface hydroxyl and adsorbed water
315 [29, 36], which is shown in Fig.5 and Table 4. It is clear evident that the ratio of O_α over
316 V(Cu)/WTi sample is much higher than that over other two samples, and the order is
317 V(Cu)/WTi>V/WTi>Cu/WTi. The result obviously indicates the chemisorbed surface
318 oxygen (O_α) content is significantly improved by Cu doping into V/WTi. The high
319 ratio of Cu^{+} over V(Cu)/WTi sample can create the charge imbalance, oxygen vacancy,

RSC Advances Accepted Manuscript

and unsaturated chemical bonds on the surface of the catalyst, contributing to more surface chemisorbed oxygen formed, which is well in accordance with the less total H_2 consumption of copper species. The surface oxygen (O_α) is more reactive in the oxidation reaction due to its higher mobility than lattice oxygen (O_β) [2, 32]. Herein, the relative higher concentration surface oxygen may be attributed to the superior NH_3-SCR activity at low temperature.

3.2.5 Surface acidity

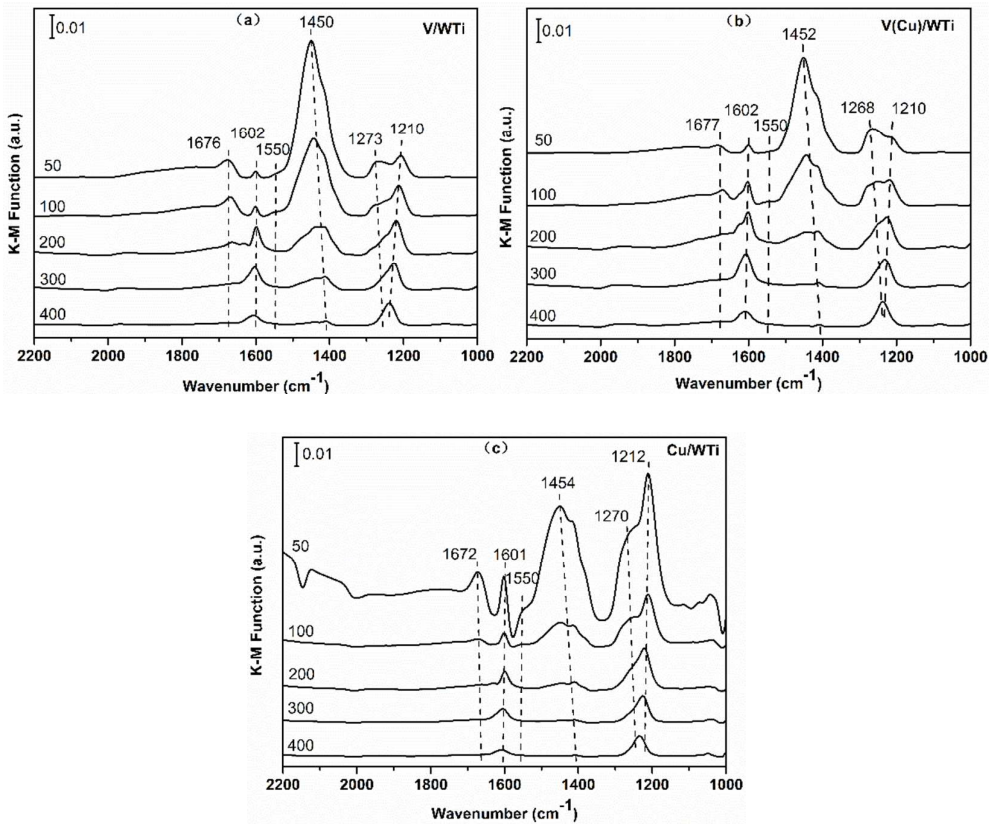

Fig.6 DRIFT spectra of NH_3 adsorption of all catalysts at different temperature

RSC Advances Accepted Manuscript

Table 5 Assignments of DRIFTS bands observed during the NH_3 adsorption.

Wavenumber (cm^{-1})	Assignments	References
1450 and 1676	asymmetric and symmetric vibrations of N-H bonds in NH_4^+ coordinately linked to Brønsted acid sites	35
1210, 1270 and 1602	asymmetric and symmetric vibrations of the coordinated NH_3 linked to Lewis acid sites	11
1550	NH_2 species coordinated to Lewis acid sites	13

Table 6 the integral of NH_3 peak area adsorbed on the Brønsted acid 1452 (cm^{-1}) and Lewis acid 1223 (cm^{-1}) at 50 ˚C.

samples	Brønsted acid （a.u.）	Lewis acid （a.u.）	L/B (a.u.)
V/WTi	9.3	1.5	0.16
V（Cu）/WTi	8.4	2.1	0.25
Cu/WTi	2.9	6.0	2.01

In order to thoroughly distinguish the Lewis acid site and Brønsted acid site and their quantities, *in situ* DRIFTS are conducted between 50 and 400 ˚C, and the results

RSC Advances Accepted Manuscript

are exhibited in Fig.6. After NH_3 adsorption on the V/WTi sample at 50 ˚C, several bands are detected in the range of 1000-1800 cm^{-1}. The bands at 1450 and 1672 cm^{-1} are assigned to asymmetric and symmetric vibrations of N-H bonds in NH_4^+ coordinately linked to Brønsted acid sites. The bands at 1602 cm^{-1} and a broaden peak between 1210 cm^{-1} and 1273 cm^{-1} are attributed to asymmetric and symmetric vibrations of the NH_3 coordinately bound to Lewis acid sites [12, 37]. In addition, amide (NH_2) species coordinated to Lewis acid sites also can be observed at 1550 cm^{-1}, which can be an important activated surface intermedia in ammonia activation for NH_3-SCR [13].

As compared with V/WTi, the results of V(Cu)/WTi and Cu/WTi are shown in Fig.6 b and c. All the similar NH_3 species adsorbed on the catalyst surface can be observed. The assignments of *in situ* DRIFTS bands are listed in Table 5. However, the intensity and proportion of these two kinds of acid sites is significant difference. In Table 6, it is clear suggesting that the V/WTi catalyst possesses the main Brønsted acid sites and the Cu/WTi catalyst contains the dominating Lewis acid sites. The proportion of Lewis acid sites on V(Cu)/WTi catalyst is slightly higher than that of the V/WTi sample, which is in accordance with the superior catalyst activity at low temperature, while the ratio of Brønsted acid sites remarkably decreases. This strongly indicates the Lewis acid sites, especially the activity of NH_3 species bonded to, play a more important role than the Brønsted acid sites in low-temperature NH_3-SCR performance.

With an increase of temperature, the intensity of the band at 1450 cm^{-1} decreases

RSC Advances Accepted Manuscript

more noticeably than that of 1210 cm^{-1}, which still remains and shifts to higher wave number. This indicates that the Lewis acid sites are more stable than Brønsted acid sites on the catalyst surface. Meanwhile, the band at 1270 cm^{-1} weakens and shifts significantly download to around 1230 cm^{-1}, which shows the weaker acid strength. It is worth noting that the peak at 1268 cm^{-1} of the V(Cu)/WTi is obviously higher than the others, which may be attributed to the large amount of lower-valent copper species due to the electron conduction between the V and Cu species decreasing the intensity of Lewis acidity [38], which is in good accordance with the EPR and TPR results. Thus the NH_3 species are mainly adsorbed on the Lewis acid site contributed from vanadium species. With the temperature increasing to 300 ˚C, all the adsorbed NH_3 species on Brønsted acid sites eventually disappear, which further indicates that the superior NH_3-SCR performance is well associated with NH_3 species bound to vanadium species in this work.

3.2.6 NO_x adsorption

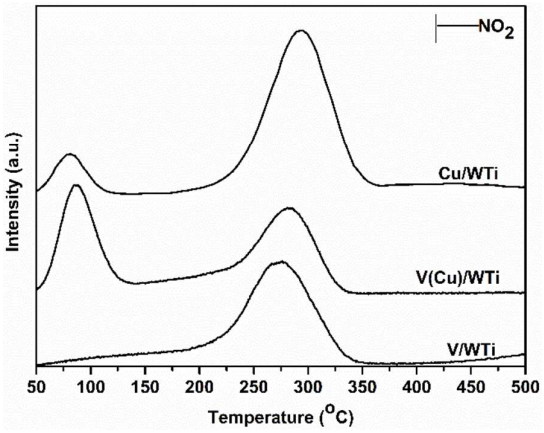

Fig.7 NO+O_2-temperature programmed desorption profiles of the obtained samples.

RSC Advances Accepted Manuscript

Table 6 The quantitative analysis of NO_2 desorbed on weak site (S_w) at 50-125 ˚C and strong site (S_s) at 200-350 ˚C.

samples	Weak site (S_w) (a.u.)	Strong site (S_s) (a.u.)	S_w / S_s	Total NO_2 amounts ($\times 10^{-3}$ mmol/g)
V/WTi	85	2,146	0.04	7.76
V（Cu）/WTi	1,024	1,715	0.60	9.12
Cu/WTi	363	3,349	0.11	12.36

The $NO+O_2$-TPD profiles of the catalysts are illustrated in Fig.7, and the quantitative results are summed in Table 6. All the catalysts show only the desorption peak of NO_2 between 50 ˚C and 350 ˚C without any desorption peak of NO, which may be due to NO oxidation by chemisorbed surface oxygen on the catalysts. Only one distinct desorption peak at 275 ˚C is observed on the V/WTi sample, whereas the Cu/WTi exhibits not only a stronger peak centered at 300 ˚C but also a small peak at 78 ˚C, respectively. The low temperature peak (labeled as Sw) can be related to the weakly adsorbed nitrate on the catalytic surface [39] and the high temperature peak (labeled as Ss) is attributed to the stably adsorbed nitrate species [8], which can be described in detail by $NO+O_2$-*in situ* DRIFTS results. This confirms that the existence of both kinds of adsorption sites over the Cu/WTi. Moreover, the amounts of the two sites are much higher than those of V/WTi. For V(Cu)/WTi samples, the first peak at 85 ˚C exhibits an obvious increase and the second peak at 285 ˚C shows a clear decrease. The ratio of Sw/Ss for V(Cu)/WTi is 0.60 much larger than the 0.11 of

RSC Advances Accepted Manuscript

Cu/WTi and 0.04 of V/WTi. From the results, it clear indicates that the addition of Cu to the V/WTi not only provides new adsorption sites but also reduces the number of strong adsorption sites, which can be explained by the synergistic interaction of electron conduction between Cu and V contributing to stably nitrate species adsorbed on Cu species transforming into weakly adsorbed ones. The large amounts of the weakly adsorbed nitrate can decompose as NO_2 with the temperature rise, which can be generally considered as an important intermediate species for NH_3-SCR in the low temperature [12, 40].

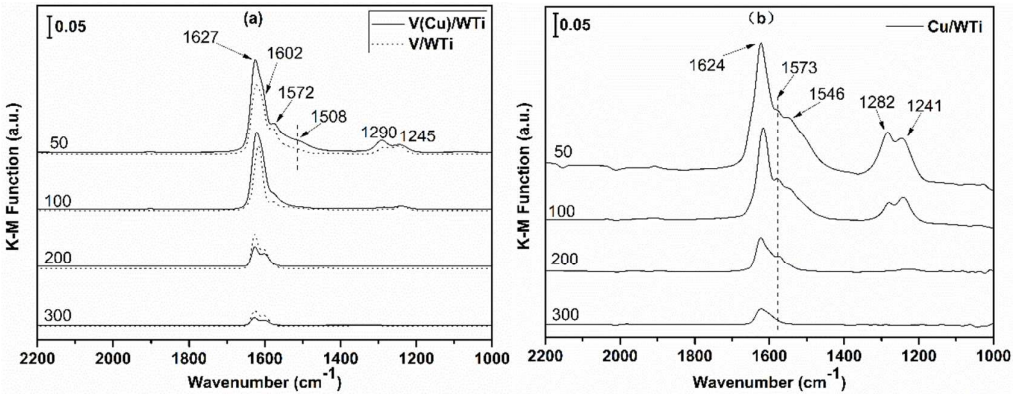

Fig.8 DRIFTS spectra of $NO+O_2$ adsorption of all catalysts at different temperature.

Table 7 Assignments of DRIFTS bands observed during the $NO+O_2$ adsorption.

Wavenumber (cm^{-1})	Assignments	References
1627	bridging bidentate nitrates	39
1603	bridging monodentate nitrates	40,41
1572	bidentate nitrates	40
1508, 1290	monodentate nitrate	41,42

RSC Advances Accepted Manuscript

1245	chelating bidentate nitrates	39

410

411 $NO+O_2$ adsorption *in situ* DRIFTS at different temperatures are shown in Fig.8.
412 For V/WTi sample, variation bands can be observed in the range of 1000-2000 cm^{-1} at
413 50 ˚C, the bands at 1627 cm^{-1} and 1245 cm^{-1} can be assigned to the N=O stretching
414 vibration of bridging bidentate nitrates and chelating bidentate nitrates [41]. The band at
415 1603 cm^{-1} and a shoulder at 1572 cm^{-1} are attributed to the bridging monodentate
416 nitrates and bidentate nitrates [42, 43]. Furthermore, the monodentate nitrates also present
417 a band at 1290 cm^{-1} [44]. With the addition of Cu, a new band at 1508 cm^{-1} attributed to
418 the monodentate nitrates appears [41]. Moreover, the intensities of all the adsorbed
419 nitrate species are much stronger, which reveals that the presence of Cu can provide
420 new adsorption sites, inducing more adsorbed nitrates species on the surface. As a
421 reference sample, all the bands of absorbed nitrates species exist on the Cu/WTi,
422 excepting for a new band at 1546 cm^{-1} attributed to the overlap of the monodentate
423 nitrate (1508 cm^{-1}) and bidentate nitrate species (1572cm^{-1}) [24]. The assignments of *in*
424 *situ* DRIFTS bands are presented in Table 7.

425 With increasing temperature to 100 ˚C, the intensities of the bands at 1572 cm^{-1},
426 1290 $cm^{-1}$and 1245 cm^{-1} remarkably decrease and the band at 1508 cm^{-1} almost
427 vanishes for V(Cu)/WTi catalyst, while those bands decrease slowly on the other
428 catalysts. This result may be due to the adsorbed nitrate species desorbing,
429 decomposing or converting into NO_2 during the heating process, which is
430 correspondence with the $NO+O_2$-TPD. With the further elevation of temperature to

RSC Advances Accepted Manuscript

300 ˚C, only the bands at 1627 cm^{-1} and 1602 cm^{-1} still exist for the three samples, which suggests the bridging bidentate and bridging monodentate nitrates are more stable. Interestingly, the intensities of the both nitrates on V(Cu)/WTi catalyst are obviously weaker than those of the other catalysts. It clear suggests the existence of Cu can significantly activate the adsorbed nitrates which are conductive to release much more NO_2 facilitating to improve the NO_2/NO_x, which is beneficial for NH_3-SCR [45].

3.2.7 Reaction between $NO+O_2$ and adsorbed NH_3 species

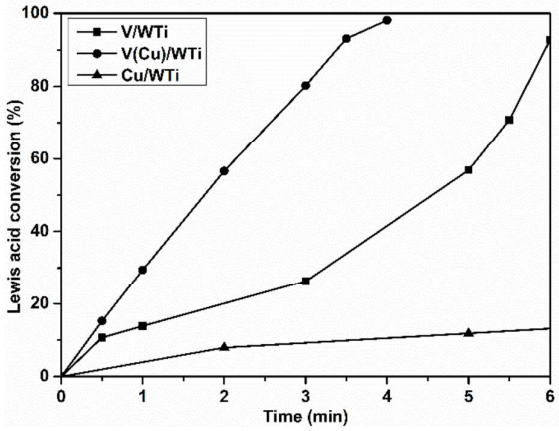

Fig.9 Integral conversion of the bands in NH_3 adsorption *in situ* DRIFTS assigned to Lewis acid site (1220 cm^{-1}) over the catalysts as a function of time at 200 ˚C.

In order to further explore the different activity of NH_3 species linked to Lewis and Brønsted acid sites on the surface of these catalysts during the NH_3-SCR process, *in situ* DRIFTS spectra of the reaction between $NO+O_2$ and pre-adsorbed NH_3 species on catalysts are recorded at 200 ˚C, and the corresponding results are shown in Fig.S2. The consumption rate of the NH_3 adsorption species linked to the Lewis sites is observably difference among the catalysts. The integral conversion of NH_3 species

RSC Advances Accepted Manuscript

adsorbed to Lewis acid site (1220 cm^{-1}) over the catalysts as a function of time at 200 ˚C is illustrated in Fig.9. It can be observed that only after 4 min the conversion of NH_3 species linked to Lewis acid sites is almost completely over V(Cu)/WTi sample, while it takes 6 min and 15 min for V/WTi and Cu/WTi to reach the same level, respectively. This demonstrates that more active NH_3 species assigned to Lewis acid site mainly attributed to surface vanadium species are formed on V(Cu)/WTi catalyst, which may be responsible for the enhancement in NH_3-SCR performance at low temperature.

3.3 **Kinetics for NH_3-SCR reaction**

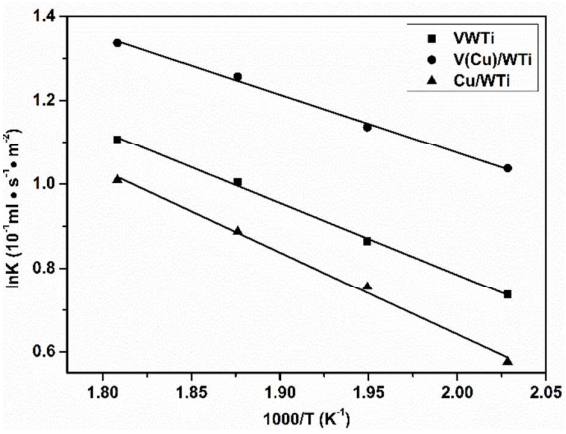

Fig.10 Arrhenius plots of intrinsic reaction rate constants of the catalysts.

Table 8 Kinetic parameter (Ea) for NH_3-SCR over the samples.

Samples	V/WTi	V(Cu)/WTi	Cu/WTi
Ea (kJ mol^{-1})	57.18	42.14	65.01

RSC Advances Accepted Manuscript

The rates of NO conversion over samples with various temperature have been plotted as an Arrhenius plot in Fig.10, and the apparent activation energies determined by the Eq. (3) are shown in Table 8. It is clear that the apparent activation energy for Cu/WTi is higher than that of V/WTi, but the V(Cu)/WTi sample shows the lowest Ea (42.14 kJ mol^{-1}). According to the kinetic results, the activation energies calculated for NH_3-SCR are in accordance with other literatures [46, 47]. Meanwhile, the same trend can be observed in normalization reaction rate constant by S_{BET} following the order as: V(Cu)/WTi> V/WTi> Cu/WTi. This result significantly indicates the decrease of Ea clear improve the rate constant well correlating with the enhancement of the redox property, which is consistent with the superior SCR activity at low temperature.

4. Discussion

4.1 The chemical modification of V/WTi by doping copper species

Our results reveal that the NH_3-SCR performance can be remarkably enhanced by Cu adding at low temperature. The XRD and Raman show that the copper and vanadium species are highly dispersed on the catalyst surface with the existence of redox couples of both V^{5+}/V^{4+} and Cu^{2+}/Cu^{+} that is proved by EPR, H_2-TPR and XPS results. Less total H_2 consumption suggests that the higher amount of Cu^{+} causes a charge imbalance on the catalyst surface, and thereby induces to generate more surface oxygen species (O_α), which benefits the enhancement of NO oxidation and the activity of weakly adsorbed nitrates on Cu species [14, 18]. It is well know that the redox properties of active sites of vanadium species play a key role in controlling the

RSC Advances Accepted Manuscript

483 performance of NH_3-SCR reaction, especially at low temperature [15, 23, 48]. The H_2-TPR
484 results reveal the copper species promote reducibility of vanadium species via the
485 transformation of V^{5+}/V^{4+}, which can be illustrated that the redox couple Cu^{+}/Cu^{2+}
486 induces electrons transfer from the reactant to V^{5+}. Besides, the existence of the redox
487 cycle of $Cu^{2+}+V^{4+}\leftrightarrow V^{5+}+Cu^{+}$ over the catalyst is also proved by XPS results and this
488 process can be described as follows [9, 29, 48, 49]:

489 $$Cu^{2+}-O^{2-}-V^{5+}+e\leftrightarrow Cu^{2+}-O^{2-}-V^{4+}\leftrightarrow Cu^{+}-O^{2-}-V^{5+}\leftrightarrow Cu^{2+}-O^{2-}-V^{5+}+e$$

490 The redox cycle can decrease the necessary energy for electrons transfer between Cu
491 and V species. The affinity of both Cu and V species promotes this process resulting
492 in the disappearance of hyperfine structure of the VO^{2+} species (Fig.3). The process
493 can significantly enhance the activity of NH_3 and NO, and therefore improve the
494 NH_3-SCR performance.

495 **4.2 The improvement of adsorption ability by doping copper species**

496 It is well known that the SCR activity is positively related to surface acid sites [50],
497 especially Lewis acid sites may be more important than Brønsted acid sites for low
498 -temperature SCR catalysts [6]. The amount of Lewis acid sites is slightly enhanced by
499 Cu additives that is one of the reasons for the enhancement of low-temperature
500 activity for our catalysts. More important, it is the NH_3 species bound to Lewis acidity
501 sties (mainly vanadium species) on V(Cu)/WTi that exhibit remarkable activity
502 among the catalyst system, which may owe to electron conduction via the redox cycle
503 of $Cu^{2+}+V^{4+}\leftrightarrow V^{5+}+Cu^{+}$. The redox cycle of $Cu^{2+}+V^{4+}\leftrightarrow V^{5+}+Cu^{+}$ shifting to right

RSC Advances Accepted Manuscript

reduces the surrounding electron clouds density of vanadium species that induces vanadium species to capture electrons from NH_3 species adsorbed on them, which contributes to the process of activing NH_3 species to form higher active -NH_2 species. Then, the reduced state of vanadium species can transfer electron to affinitive Cu species via the redox cycle. This process can significantly decrease the reactive energy barrier conducing to the lowest Ea for NH_3-SCR. On the other hand, the NO+O_2-TPD and *in situ* DRIFTS suggest that the addition of Cu increases NO_x species adsorption sites and therefor the amount of nitrates. Meanwhile, the presence of Cu^+ species via the redox cycle induces a charge imbalance so that more surface oxygen species (O_α) are formed around the Cu species, which significantly improves the activity of nitrates adsorbed on surface Cu species and thereby results in more NO_2 release. Therefore, the higher active NH_3 species mainly bonded to V species and active surface nitrates adsorbed on Cu species are responsible for the excellent NH_3-SCR performance.

4.3 Possible mechanism of the improvement of NH_3-SCR over V(Cu)/WTi catalyst

Our results indicate that the reaction process of NH_3-SCR on all the catalysts follows the same Eley-Rideal mechanism (Fig.S5). But redox properties may be a main factor that is closely related to the reactivity of NH_3-SCR at low temperature in our present work, which can be well explained by results of kinetics. The lowest activation energy achieved during the NH_3-SCR process over the V(Cu)/WTi catalyst supports our hypothesis.

RSC Advances Accepted Manuscript

Based on above discussions, the possible promotion process of NH_3-SCR reaction is then exhibited in Scheme.1. The interaction between surface vanadium and copper oxide sites by electrons transfer ($Cu^{2+}+V^{4+}\leftrightarrow V^{5+}+Cu^{+}$) may promote the adsorption and activity of NH_3 species linked to vanadium species (Fig.9 and Fig.S2). Besides, the existence of numerous Cu^{+} species induces more surface oxygen species (O_α) formation, which facilitates the activity of weak adsorption nitrates on Cu species. More NO_2 is released from these high active nitrates and promotes the fast NH_3-SCR [12]. Therefore, it is the redox cycle of Cu and V species ($Cu^{2+}+V^{4+}\leftrightarrow V^{5+}+Cu^{+}$) that improves the NH_3-SCR on V(Cu)/WTi at low temperature.

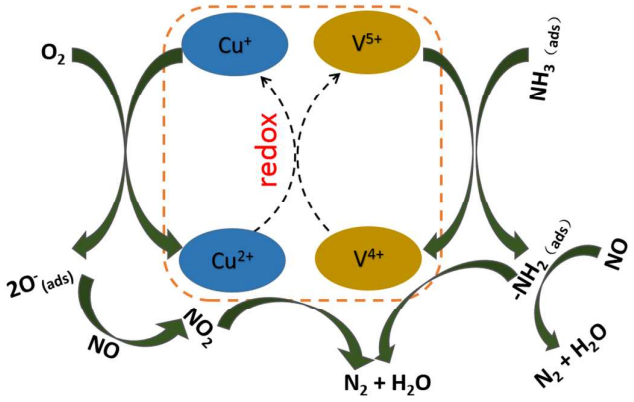

Scheme.1 Possible mechanism of the improvement of NH_3-SCR over V(Cu)/WTi catalyst.

5. Conclusions

In this work, the promoting effect of Cu for NH_3-SCR was intensively investigated. The presence of Cu enhances the redox property of Vanadium via the redox cycle of $Cu^{2+}+V^{4+}\leftrightarrow V^{5+}+Cu^{+}$, which remarkably increases the activity of NH_3 species adsorbed on vanadium species. Meanwhile, the redox cycle can not only provide more adsorbed nitrate sites but conduce to form higher activity nitrates

RSC Advances Accepted Manuscript

543 species on copper species of the catalyst. The higher level of surface oxygen species
544 (O_α) is beneficial to form NO_2, which also contributes to the excellent NH_3-SCR
545 performance at low temperature. Consequently, the electron conduction via redox
546 cycle of $Cu^{2+}+V^{4+}\leftrightarrow V^{5+}+Cu^{+}$ significantly decreases the Ea for NH_3-SCR at low
547 temperature, facilitating the low-temperature activity.

548 **Acknowledgements**

549 The authors acknowledge the China Huadian Science and Technology Institute
550 (CHDI.KJ-20) for financial support. This work is supported by the program of the
551 National High Technology Research and Development Program if China (863
552 Program, 2011AA03A405).

553 **Notes and references**

554 1 P. Forzatti, I. Nova and E. Tronconi, *Angew. Chem. Int. Ed. Engl*, 2009, **48**,
555 8366-8368.
556 2. M. S. Maqbool, A. K. Pullur and H. P. Ha, *Appl. Catal., B*, 2014, **152**, 28-37.
557 3. Y. Li, H. Cheng, D. Li, Y. Qin, Y. Xie and S. Wang, *Chem Commun (Camb)*,
558 2008, 1470-1472.
559 4. R. Jin, Y. Liu, Y. Wang, W. Cen, Z. Wu, H. Wang and X. Weng, *Appl. Catal., B*,
560 2014, **148-149**, 582-588.
561 5. B. Thirupathi and P. G. Smirniotis, *J. Catal.*, 2012, **288**, 74-83.
562 6. P. G. Smirniotis, D. A. Peña and B. S. Uphade, *Angew. Chem. Int. Ed.*, 2001,

RSC Advances Accepted Manuscript

40, 2479-2482.

7. P. R. Ettireddy, A. Kotrba, T. Spinks, T. Boningari and P. Smirniotis, *Development of Low Temperature Selective Catalytic Reduction (SCR) Catalysts for Future Emissions Regulations*, SAE Technical Paper, 2014.

8. R. Gao, D. Zhang, X. Liu, L. Shi, P. Maitarad, H. Li, J. Zhang and W. Cao, *Catal. Sci. Technol.*, 2013, **3**, 191-199.

9. Z. Liu, Y. Li, T. Zhu, H. Su and J. Zhu, *Ind. Eng. Chem. Res.*, 2014, **53**, 12964-12970.

10. P. G. W. A. Kompio, A. Brückner, F. Hipler, G. Auer, E. Löffler and W. Grünert, *J. Catal.*, 2012, **286**, 237-247.

11. H.-L. Koh and H.-K. Park, *J. Ind. Eng. Chem.*, 2013, **19**, 73-79.

12. L. Chen, Z. Si, X. Wu and D. Weng, *ACS Appl Mater Interfaces*, 2014, **6**, 8134-8145.

13. G. Ramis, L. Yi, G. Busca, M. Turco, E. Kotur and R. J. Willey, *J. Catal.*, 1995, **157**, 523-535.

14. L. J. Alemany, L. Lietti, N. Ferlazzo, P. Forzatti, G. Busca, E. Giamello and F. Bregani, *J. Catal.*, 1995, **155**, 117-130.

15. I. E. Wachs, G. Deo, B. M. Weckhuysen, A. Andreini, M. A. Vuurman, M. d. Boer and M. D. Amiridis, *J. Catal.*, 1996, **161**, 211-221.

16. M. D. Amiridis, I. E. Wachs, G. Deo, J.-M. Jehng and D. S. Kim, *J. Catal.*, 1996, **161**, 247-253.

17. J. A. Dumesic, N. Y. Topsøe, H. Topsøe, Y. Chen and T. Slabiak, *J. Catal.*,

RSC Advances Accepted Manuscript

1996, **163**, 409-417.

18. L. Lietti, I. Nova, S. Camurri, E. Tronconi and P. Forzatti, *AlChE J.*, 1997, **43**, 2559-2570.

19. I. E. Wachs, G. Deo, B. M. Weckhuysen, A. Andreini, M. A. Vuurman, M. d. Boer and M. D. Amiridis, *J. Catal.*, 1996, **161**, 211-221.

20. M. C. Paganini, L. Dall'Acqua, E. Giamello, L. Lietti, P. Forzatti and G. Busca, *J. Catal.*, 1997, **166**, 195-205.

21. A. Brückner, U. Bentrup and J.-B. Stelzer, *Z. Anorg. Allg. Chem.*, 2005, **631**, 60-66.

22. S. T. Martin, C. L. Morrison and M. R. Hoffmann, *The Journal of Physical Chemistry*, 1994, **98**, 13695-13704.

23. J. Xue, X. Wang, G. Qi, J. Wang, M. Shen and W. Li, *J. Catal.*, 2013, **297**, 56-64.

24. X. Wang, A. Shi, Y. Duan, J. Wang and M. Shen, *Catal. Sci. Technol.*, 2012, **2**, 1386-1395.

25. S. M. Jung and P. Grange, *Appl. Catal., B*, 2001, **32**, 123-131.

26. L. Chen, J. Li and M. Ge, *The Journal of Physical Chemistry C*, 2009, **113**, 21177-21184.

27. S. M. Lee and S. C. Hong, *Appl. Catal., B*, 2015, **163**, 30-39.

28. S. Besselmann, C. Freitag, O. Hinrichsen and M. Muhler, *PCCP*, 2001, **3**, 4633-4638.

29. X. Yao, L. Zhang, L. Li, L. Liu, Y. Cao, X. Dong, F. Gao, Y. Deng, C. Tang, Z.

RSC Advances Accepted Manuscript

Chen, L. Dong and Y. Chen, *Appl. Catal., B*, 2014, **150–151**, 315-329.

30. H. Zhu, L. Dong and Y. Chen, *J. Colloid Interface Sci.*, 2011, **357**, 497-503.

31. J. Mendialdua, R. Casanova and Y. Barbaux, *J. Electron. Spectrosc. Relat. Phenom.*, 1995, **71**, 249-261.

32. J. Y. Lee, S. H. Hong, S. P. Cho and S. C. Hong, *Curr. Appl Phys.*, 2006, **6**, 996-1001.

33. X. Guo, C. Bartholomew, W. Hecker and L. L. Baxter, *Appl. Catal., B*, 2009, **92**, 30-40.

34. H. Zhu, M. Shen, Y. Kong, J. Hong, Y. Hu, T. Liu, L. Dong, Y. Chen, C. Jian and Z. Liu, *J. Mol. Catal. A: Chem.*, 2004, **219**, 155-164.

35. B. Liu, J. Du, X. Lv, Y. Qiu and C. Tao, *Catal. Sci. Technol.*, 2014.

36. M. Kang, E. D. Park, J. M. Kim and J. E. Yie, *Appl. Catal., A*, 2007, **327**, 261-269.

37. N. Y. Topsoe, H. Topsoe and J. A. Dumesic, *J. Catal.*, 1995, **151**, 226-240.

38. Z. Si, D. Weng, X. Wu, J. Li and G. Li, *J. Catal.*, 2010, **271**, 43-51.

39. R. Jin, Y. Liu, Z. Wu, H. Wang and T. Gu, *Catal. Today*, 2010, **153**, 84-89.

40. M. Koebel, G. Madia, F. Raimondi and A. Wokaun, *J. Catal.*, 2002, **209**, 159-165.

41. K. I. Hadjiivanov, *Catal. Rev.*, 2000, **42**, 71-144.

42. X. Yao, Q. Yu, Z. Ji, Y. Lv, Y. Cao, C. Tang, F. Gao, L. Dong and Y. Chen, *Appl. Catal., B*, 2013, **130–131**, 293-304.

43. A. Trovarelli, *Catal. Rev.*, 1996, **38**, 439-520.

RSC Advances Accepted Manuscript

44. T. Gu, R. Jin, Y. Liu, H. Liu, X. Weng and Z. Wu, *Appl. Catal., B*, 2013, **129**, 30-38.

45. W. Zhao, Q. Zhong, T. Zhang and Y. Pan, *RSC Adv.*, 2012, **2**, 7906.

46. A. Shi, X. Wang, T. Yu and M. Shen, *Appl. Catal., B*, 2011, **106**, 359-369.

47. M. Iwasaki, in *Urea-SCR Technology for deNOx After Treatment of Diesel Exhausts*, Springer, 2014, pp. 221-246.

48. Z. Liu, Y. Yi, J. Li, S. I. Woo, B. Wang, X. Cao and Z. Li, *Chem. Commun.*, 2013, **49**, 7726-7728.

49. Z. Liu, S. Zhang, J. Li, J. Zhu and L. Ma, *Appl. Catal., B*, 2014, **158–159**, 11-19.

50. C.-H. Lin and H. Bai, *Appl. Catal., B*, 2003, **42**, 279-287.

RSC Advances Accepted Manuscript